ISSN 1674-1056
http://cpb.iphy.ac.cn
http://iopscience.iop.org/cpb
中国物理 B
Chinese Physics
中国物理 Chinese Physics B

Physical properties of ternary thallium chalcogenes Tl_2MQ_3 (M=Zr, Hf; Q=S, Se, Te) via *ab-initio* calculations

Engin Ateser[1], Oguzhan Okvuran[1], Yasemin Oztekin Ciftci[2], Haci Ozisik[1], Engin Deligoz[1]

Citation: Chin. Phys. B . 2019, 28(10): 106301 . **doi:** 10.1088/1674-1056/ab427d
Journal homepage: http://cpb.iphy.ac.cn; http://iopscience.iop.org/cpb

What follows is a list of articles you may be interested in

First-principles study of structural, mechanical, and electronic properties of W alloying with Zr

Ning-Ning Zhang(张宁宁), Yu-Juan Zhang(张玉娟), Yu Yang(杨宇), Ping Zhang(张平), Chang-Chun Ge(葛昌纯)
Chin. Phys. B . 2019, 28(4): 046301 . **doi:** 10.1088/1674-1056/28/4/046301

Electronic structures and optical properties of Si- and Sn-doped β-Ga_2O_3: A GGA+U study

Jun-Ning Dang(党俊宁), Shu-wen Zheng(郑树文), Lang Chen(陈浪), Tao Zheng(郑涛)
Chin. Phys. B . 2019, 28(1): 016301 . **doi:** 10.1088/1674-1056/28/1/016301

First-principles study of the $(Cu_xNi_{1-x})_3Sn$ precipitations with different structures in Cu-Ni-Sn alloys

Guang-Wei Peng(彭广威), Xue-Ping Gan(甘雪萍), Zhou Li(李周), Ke-Chao Zhou(周科朝)
Chin. Phys. B . 2018, 27(8): 086302 . **doi:** 10.1088/1674-1056/27/8/086302

First principles study of ceramic materials (IVB group carbides) under ultrafast laser irradiation

Nan-Lin He(何南燐), Xin-Lu Cheng(程新路), Hong Zhang(张红), Gai-Qin Yan(闫改琴), Jia Zhang(张佳)
Chin. Phys. B . 2018, 27(3): 036301 . **doi:** 10.1088/1674-1056/27/3/036301

Magnetism and piezoelectricity of hexagonal boron nitride with triangular vacancy

Lu-Si Zhao(赵路丝), Chun-Ping Chen(陈春平), Lin-Lin Liu(刘林林), Hong-Xia Yu(于洪侠), Yi Chen(陈怡), Xiao-Chun Wang(王晓春)
Chin. Phys. B . 2018, 27(1): 016301 . **doi:** 10.1088/1674-1056/27/1/016301

Physical properties of ternary thallium chalcogenes Tl_2MQ_3 (M = Zr, Hf; Q = S, Se, Te) via *ab-initio* calculations

Engin Ateser[1,†], Oguzhan Okvuran[1], Yasemin Oztekin Ciftci[2], Haci Ozisik[1], and Engin Deligoz[1]

[1] *Aksaray University, Department of Physics*, 68100, *Aksaray, Turkey*
[2] *Gazi University, Science Faculty, Physics Department*, 06500, *Ankara, Turkey*

(Received 8 November 2018; revised manuscript received 18 August 2019; published online 30 September 2019)

We have reported a first principles study of structural, mechanical, electronic, and thermoelectric properties of the monoclinic ternary thallium chalcogenes Tl_2MQ_3 (M = Zr, Hf; Q = S, Se, Te). The electronic band structure calculations confirm that all compounds exhibit semiconductor character. Especially, Tl_2ZrTe_3 and Tl_2HfTe_3 can be good candidates for thermoelectric materials, having narrow band gaps of 0.169 eV and 0.21 eV, respectively. All of the compounds are soft and brittle according to the second-order elastic constant calculations. Low Debye temperatures also support the softness. We have obtained the transport properties of the compounds by using rigid band and constant relaxation time approximations in the context of Boltzmann transport theory. The results show that the compounds could be considered for room temperature thermoelectric applications ($ZT \sim 0.9$).

Keywords: electronic band structure, thermoelectric properties, figure of merit, ternary thallium chalcogens

PACS: 63.20.dk, 74.25.Ld, 74.25.F– **DOI:** 10.1088/1674-1056/ab427d

1. Introduction

Recent studies about chalcogens have a variety of applications such as energy, magnetism, superconductivity, electronics, optoelectronics, and catalysis.[1–8] One of the popular topics within these is thermoelectricity, generating electricity by converting the temperature difference to an electrical voltage. For energy management in this way, the thermoelectric materials (TEM) become indispensable. As it is known that, the accomplishment of TEM addresses to dimensionless figure of merit (ZT) which is directly proportional to the power factor ($S^2\sigma$; S, Seebeck coefficient and σ, electrical conductivity), and inversely proportional to the thermal conductivity (k). Since some of the efficient TEM are narrow band semiconductor chalcogenides and antimonides with heavy and complex structures,[9,10] there are many theoretical and experimental studies on them to advance TEM. While various efforts have concentrated on getting a higher power factor, the others have centered on decreasing the lattice thermal conductivity. One of the ways of Seebeck coefficient enhancement is alloying. For example, in Refs. [11]– [13], Mg and Cd were integrated to SnTe and PbSe, respectively, in order to have more carrier contribution from Σ (heavy) to L (light) hole valance bands by reducing the energy gap between them. Another way of Seebeck coefficient improvement is stoichiometry, e.g., in Ref. [14], the TEM properties of $Tl_{10-x}Sn_xTe_6$ and $Tl_{10-x}Pb_xTe_6$ were examined as a function of x varying between 1.8 and 2.06 and $ZT_{max} > 1$ (commercially viable value) was obtained. The difficulty of ZT improvement is the interconnection of S, σ, and k. Therefore, they tried to have a higher S while keeping σ unchanged. The strategy was to increase the number of valence electrons which decreases the dominating p-type charge carriers. So a larger Seebeck coefficient could be achieved while leaving the thermal conductivity remained under 0.5 W/m/K. Li *et al.* have made a pioneering review about introducing some new scattering mechanisms for ZT enhancement via nanostructures in the bulk materials hindering the interconnection of the thermal and electrical transports.[15] Meanwhile, several methodologies have been applied to reduce the lattice thermal conductivity, such as strengthening the phonon scattering.[16–21] Phonon scattering, produced by point defects in Ref. [16] and accommodation of metal cations in Ref. [17], is responsible for having a reduced lattice thermal conductivity. The mass and strain fluctuations between host and guest atoms, which produces strong phonon scattering, could also be maximized by vacancies as demonstrated in Ref. [18]. Furthermore, the substitution of Zn and Sn atoms in the disordered Sb/Se site caused an improved power factor, resulting in the maximum ZT of 0.53 at 657 K. in Ref. [16]. It is known that heterostructures on the nanoscale may decrease the thermal conductivity while improving the electronic properties, thereby increasing the ZT value as shown in Ref. [19].

Especially, thallium containing chalcogenides are candidates of narrow band gap semiconductors because of their high atomic weight and so complex structure. Also, the high electronegativity of Tl compared to that of the other alkali metal ions is important for the band gap. Furthermore, it is also important that the presence of a lone pair in Tl^+ ions causes anharmonicity in the lattice which has a remarkable effect on lowering the lattice thermal conductivity.[22–29] $Tl_2Ag_{12}Se_7$, a new pnp conduction switching semiconductor ($E_g = 0.8$ eV) has just been synthesized, possessing a new structure type, namely, $a\sqrt{3} \times \sqrt{3} \times 1$ super cell of the $Zr_2Fe_{12}P_7$-type,[23] P-type polycrystalline thallium lanthanides Tl_9LnTe_6 (Ln = La,

†Corresponding author. E-mail: enginateser4@hotmail.com

© 2019 Chinese Physical Society and IOP Publishing Ltd

Ce, Pr, Nd, Sm, Gd, Tb) and $Tl_{10-x}La_xTe_6$ ($0.90 \leq x \leq 1.05$) were synthesized. The ZT value was improved by using different lanthanides and changing the load concentrations.[24] The ZT values for TlSbTe, Tl_9BiTe_6, Tl_4ZrTe_4, and Tl_4HfTe_4 compounds were 0.87 at 715 K, 1.2 at 500 K, 0.16 at 420 K, and 0.09 at 540 K, respectively.[26,27] Sankar *et al.* firstly synthesized Tl_2ZrSe_3 (cubic, $P2_13$ space group) and found $ZT = 0.18$ at 420 K for Tl_2ZrTe_3, $ZT = 0.31$ at 500 K for Tl_2SnTe_3.[28] Later, they synthesized Tl_2MQ_3 ($M =$ Zr, Hf, $Q =$ S, Se) which have a new isostructural monoclinic structure with $P2_1$/m space group.[29] They have also studied their crystallographic features, electronic structures, and electrical conductivity.

Using the density functional theory (DFT), we systematically investigate the structural, electronic, mechanic, and thermoelectric properties of Tl_2HfS_3,Tl_2HfSe_3,Tl_2HfTe_3, Tl_2ZrS_3, Tl_2ZrSe_3, and Tl_2ZrTe_3 compounds for the first time. We have also added new additional data by comparing them with the previous studies. The organization of this study is as follows. The method of calculation is given in Section 2, the results and overall conclusions are presented and discussed in Sections 3 and 4.

2. Method of calculation

All calculations have been accomplished by using the Vienna *ab initio* simulation package (VASP)[30–33] based on the density functional theory (DFT). The electron–ion interaction was considered in the form of the projector-augmented-wave (PAW) method with plane waves up to an energy of 450 eV,[33,34] an adequate value for studying the structural, elastic, and lattice dynamical properties. Perdew–Burke–Ernzerhof (PBE) type functional[35] within the generalized gradient approximation (GGA) has been used for the exchange and correlation terms in the electron–electron interaction. $17 \times 17 \times 13$ Γ-centered Monkhorst–Pack[36] grid of k-points has been used for these monoclinic compounds.

To obtain the transport properties of Tl_2MQ_3 ($M =$ Zr, Hf; $Q =$ S, Se, Te) compounds, we have used the rigid-band approximation and semiclassical Boltzmann theory using BoltzTraP code.[37] For the calculations of transport coefficients (electrical conductivity σ, thermopower S, and electronic contribution of thermal conductivity k_e), we need to calculate the velocities as a function of k for different bands. To get accurate electronic velocities, it is necessary to have a dense k-points mesh.[38] For this reason, we used $34 \times 34 \times 26$ Monkhorst–Pack k-points sampling to obtain the band structure.

3. Results and discussion

3.1. Structural properties

We assume that the compounds Tl_2MQ_3 ($M =$ Zr, Hf; $Q =$ S, Se, Te) crystalize in monoclinic structure, similar to Na_2FeO_3-type, with $P2_1/m$ space group, as were synthesized in Ref. [29]. Their general crystal arrangement can be seen in Fig. 1 having 12 atoms occupying 2e (x, z) site in the unit cell ($Z = 2$) given in Table 1.

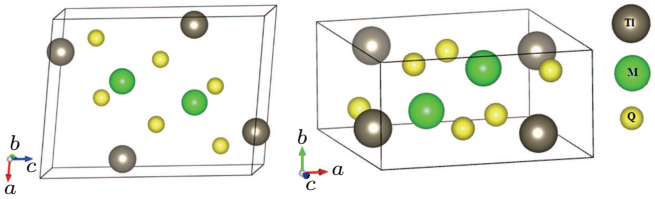


Fig. 1. Unit cell arrangement of the Tl_2MQ_3 compounds with Na_2FeO_3-type structure.

Table 1. The calculated atomic positions for Tl_2MQ_3 ($M =$ Zr, Hf; $Q =$ S, Se, Te) compounds (All of them are in 2e (x, 1/4, z) wyckoff positions).

Compound	Atom	x	z	Ref.	Compound	Atom	x	z	Ref.
Tl_2ZrS_3	Tl1	0.06444	0.65755	present	Tl_2HfS_3	Tl1	0.06171	0.65820	present
		0.06374	0.66029	Exp.[29]		Tl2	0.74584	0.98982	present
	Tl2	0.74519	0.99169	present		Hf	0.41420	0.33995	present
		0.75009	0.00227	Exp.[29]		S1	0.14146	0.20003	present
	Zr	0.41287	0.33828	present		S2	0.45484	0.77661	present
		0.41111	0.33548	Exp.[29]		S3	0.68425	0.51687	present
	S1	0.13803	0.19800	present	Tl_2HfSe_3	Tl1	0.06439	0.65512	present
		0.13620	0.19270	Exp.[29]			0.06445	0.65805	Exp.[29]
	S2	0.45252	0.78083	present		Tl2	0.74433	0.99267	present
		0.45650	0.78680	Exp.[29]			0.74973	0.00293	Exp.[29]
	S3	0.68777	0.51615	present		Hf	0.40988	0.33667	present
		0.68880	0.51506	Exp.[29]			0.40960	0.33423	Exp.[29]
Tl_2ZrSe_3	Tl1	0.06630	0.65468	present		Se1	0.13323	0.19602	present
	Tl2	0.74286	0.99422	present			0.13036	0.19044	Exp.[29]
	Zr	0.40828	0.33511	present		Se2	0.45006	0.78219	present
	Se1	0.12987	0.19383	present			0.45271	0.78917	Exp.[29]
	Se2	0.44756	0.78583	present		Se3	0.68854	0.51489	present
	Se3	0.69213	0.51429	present			0.69076	0.51355	Exp.[29]
Tl_2ZrTe_3	Tl1	0.06642	0.64949	present	Tl_2HfTe_3	Tl1	0.06594	0.64938	present
	Tl2	0.73944	0.99555	present		Tl2	0.74184	0.99473	present
	Zr	0.40439	0.32996	present		Hf	0.40608	0.33119	present
	Te1	0.11789	0.18901	present		Te1	0.12096	0.19129	present
	Te2	0.43834	0.79280	present		Te2	0.44097	0.78994	present
	Te3	0.69469	0.51228	present		Te3	0.69097	0.51299	present

We have fully optimized the lattice constants and ionic positions by taking the experimental values from Ref. [29]. The obtained equilibrium lattice parameters, volumes, and total energies are listed in Table 2. It is seen that the lattice parameters are in good agreement with the experimental values[29] and a bit higher than them as expected due to the theoretical calculations.

Table 2. Calculated equilibrium lattice parameters (a, b, and c in Å), the angle (β in degree), total energies (E_0, eV/f.u.), formation enthalpy (ΔH_f, eV/atom), and volumes (V_0, Å^3) of the Tl_2MQ_3 (M = Zr, Hf; Q = S, Se, Te) compounds.

Compound	a	b	c	β	E_0	ΔH_f	V_0	Ref.
Tl_2ZrS_3	7.940	3.818	10.559	96.9	–31.302	–1.568	158.9	present
	7.916	3.765	10.276	97.5			151.8	Exp.[29]
Tl_2ZrSe_3	8.168	3.967	10.916	96.4	–28.849	–1.212	175.7	present
Tl_2ZrTe_3	8.528	4.227	11.550	95.4	–26.028	–0.775	207.2	present
							194.1	Exp. Cubic[28]
Tl_2HfS_3	7.979	3.775	10.580	97.6	–32.885	–1.603	157.9	present
Tl_2HfSe_3	8.211	3.931	10.927	97.0	–30.282	–1.222	175.0	present
	8.154	3.881	10.622	97.4			166.7	Exp.[29]
Tl_2HfTe_3	8.568	4.208	11.536	95.9	–27.300	–0.758	206.9	present

The thermal stability is calculated by using the formation enthalpy expression. Formation enthalpy ΔH is required for the quantitative evaluation of the structural stability of materials. To determine the stability of the Tl_2MQ_3 compounds crystallized in monoclinic structure, we have calculated ΔH by using the following expression:

$$\Delta H^{Tl_2MQ_3} = E_{tot}^{Tl_2MQ_3} - 2E_t^{Tl} - E_t^M - 3E_t^Q. \quad (1)$$

Here $E_{tot}^{Tl_2MQ_3}$ is the total energy of Tl_2MQ_3 per unit cell, and $2E_t^{Tl}$, E_t^M, and E_t^Q represent the computed energies per unit cell at the absolute temperature for Tl, M, and Q, respectively. Generally, if ΔH is negative, then the material is considered to be energetically favorable to be synthesized experimentally. The computed formation enthalpies of these compounds are between -0.758 and -1.603 eV/unit cell for Tl_2MQ_3 (see Table 2). The negative values of ΔH confirm the stabilities of these materials, and Tl_2HfS_3 is the most stable one among the Tl_2MQ_3 (M = Zr, Hf; Q = S, Se, Te) compounds due to the higher magnitude of ΔH.

3.2. Electronic properties

The electronic band calculations have been performed for the titled compounds in monoclinic $P2_1/m$ structure, and the band structures of each compound along the high symmetry points are shown with the density of states in Figs. 2 and 3, where the Fermi energy level is taken as $E_F = 0$ for convenience.

As shown in Figs. 2 and 3, all compounds in the considered phase exhibit semiconductor character due to the total density of states, which are compatible with the band structures. While the Tl_2ZrS_3 compound has a direct band gap, the others have indirect band gaps. As the atomic weight of the chalcogens increases from S, Se to Te, the band gap changes as follows: Te-containing compounds with (~ 0.15 eV), Se-containing compounds with (~ 0.60 eV), and S-containing compounds with (~ 0.90 eV). It is observed that there are indirect transitions as well as direct transactions having very close ($\Delta E_g \sim 0.1$ eV) energy values of the indirect ones (see Table 3). In spite that indirect (direct) transitions are fundamental, secondary ones are direct (indirect) possessing a bit energy differences ($\Delta E_g \sim 0.1$ eV). It is known that, GGA-PBE estimates lower band gap values than the experimental ones. Although, the value computed for the Tl_2ZrS_3 compound is being fit the expectations, the calculated band gap for Tl_2HfSe_3 is higher than the value found in the experiment.[29] We have also verified the influence of HSE06 on the electronic properties by employing GGA + HSE06 functional for Tl_2HfSe_3 and have observed that the band gap energies increase by nearly 90%. But, it can be seen from Table 3 that the band gap value for GGA is very close to the experimental value for Tl_2HfSe_3. So we did not use the GGA + HSE06 functional.

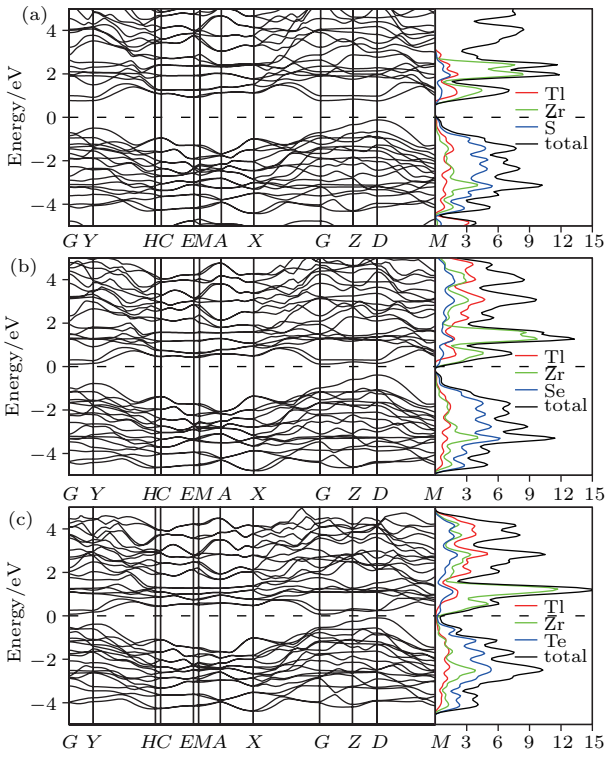


Fig. 2. The electronic band structure and density of states for (a) Tl_2ZrS_3, (b) Tl_2ZrSe_3, and (c) Tl_2ZrTe_3.

The total and projected densities of states of the studied compounds have been calculated and shown in Figs. 2 and 3. It can be found that while Q (S, Se, and Te) elements are

dominant in the conduction band, the leading elements of the valance band are *M* (Hf and Zr).

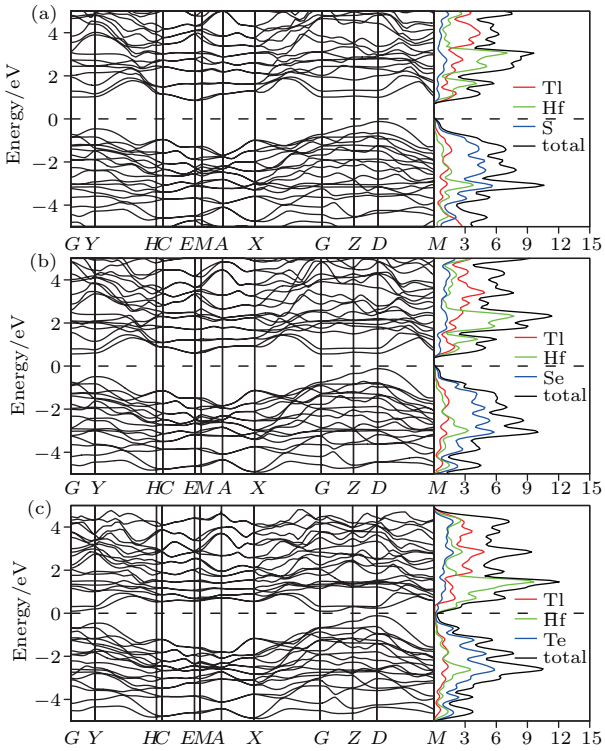


Fig. 3. The electronic band structure and density of states for (a) Tl_2HfS_3, (b) Tl_2HfSe_3, and (c) Tl_2HfTe_3.

We have also considered the electronic charge densities of the related compounds for $(0\bar{1}0)$ and $(1\bar{1}\bar{2})$ faces to estimate the bonding mechanism, as seen in Figs. 4 and 5 for Tl_2HfS_3, Tl_2ZrS_3, and Tl_2ZrSe_3 compounds on $(0\bar{1}0)$ and Tl_2HfTe_3 and Tl_2ZrTe_3 compounds on $(1\bar{1}\bar{2})$. It can be seen that the contribution to binding is more ionic than covalent.

Table 3. The calculated band gaps and for Tl_2ZrS_3, Tl_2ZrSe_3, Tl_2ZrTe_3, Tl_2HfS_3, Tl_2HfSe_3, and Tl_2HfTe_3 compounds.

Compound	E_g/eV	Type	Ref.
Tl_2ZrS_3	0.87	direct (D→D)	present
		indirect (D→ Γ−Y)	present
	0.88	indirect (D→ Γ)	present
	1.15	direct (D→D)	Exp.[26]
Tl_2ZrSe_3	0.50	indirect (D→ Γ−Y)	present
	0.54	direct (D→D)	present
Tl_2ZrTe_3	0.169	indirect (D→ Γ−Y)	present
	0.179	indirect (D→Y)	present
	0.185	direct (D→D)	present
	0.7		Ref. [28]
Tl_2HfS_3	0.975	indirect (D→E)	present
	0.990	direct (D→D)	present
Tl_2HfSe_3	0.68	indirect (D→ Γ)	present
	0.71	direct (D→D)	present
	1.19	indirect (D→ Γ)	present (HSE06)
	1.20	direct (D→D)	present (HSE06)
	0.57	direct (D→D)	Exp.[29]
Tl_2HfTe_3	0.21	indirect (D→ Γ)	present
	0.23	direct (D→D)	present

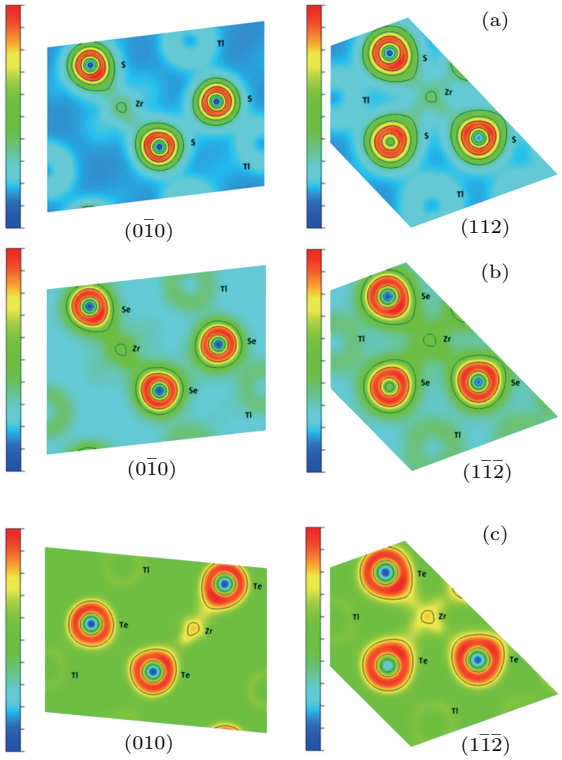


Fig. 4. The contour plot of charge density for (a) Tl_2ZrS_3, (b) Tl_2ZrSe_3, and (c) Tl_2ZrTe_3.

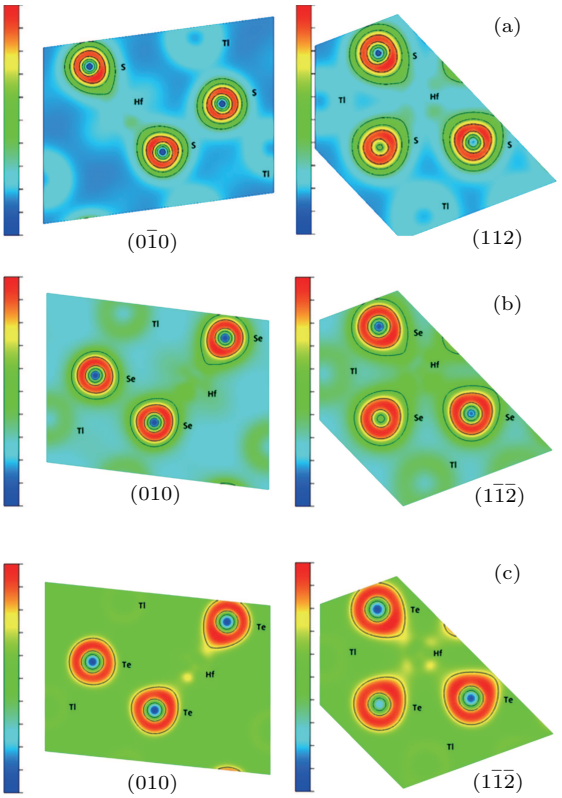


Fig. 5. The contour plot of charge density for (a) Tl_2HfS_3, (b) Tl_2HfSe_3, and (c) Tl_2HfTe_3.

3.3. Mechanical properties

3.3.1. Elastic properties

An elastic tensor provides the description of all the responses of a crystal to external forces within the elastic lim-

its. It is one of the fundamental properties that explain the interatomic bonding in a system, and can be correlated with many mechanical, thermal properties for searching process of new material's discovery and design.[35] We have computed the second order elastic constants (C_{ij}) using the stress–strain methodology embedded in VASP.[30] The calculated C_{ij} for the titled compounds shown in Table 4 obey the mechanical stability conditions for monoclinic structures given below:

$$C_{11} > 0,\ C_{22} > 0,\ C_{33} > 0,\ C_{44} > 0,\ C_{55} > 0,\ C_{66} > 0,$$
$$[C_{11} + C_{22} + C_{33} + 2(C_{12} + C_{13} + C_{23})] > 0,$$
$$\left(C_{33}C_{55} - C_{35}^2\right) > 0 (C_{44}C_{66} - C_{46}^2) > 0,$$
$$(C_{22} + C_{33} - 2C_{23}) > 0.$$

Unfortunately, the experimental values of C_{ij} are not available at present.

Table 4. The calculated elastic constants (C_{ij}, GPa) for Tl_2MQ_3 (M = Zr, Hf; Q = S, Se, Te).

Comp.	C_{11}	C_{22}	C_{33}	C_{44}	C_{55}	C_{66}	C_{12}	C_{13}	C_{15}	C_{23}	C_{25}	C_{35}	C_{46}
Tl_2HfS_3	52.3	77.0	26.2	12.7	15.0	12.1	10.7	12.7	–4.0	9.9	–6.7	–2.2	–4.1
Tl_2HfSe_3	47.7	64.3	28.4	14.6	16.0	13.0	11.0	12.8	–3.8	11.5	–7.3	–1.4	–5.1
Tl_2HfTe_3	38.9	50.2	30.5	16.4	17.2	13.1	10.4	13.1	–4.4	13.7	–7.8	–0.3	–7.0
Tl_2ZrS_3	53.4	72.8	29.4	14.7	16.0	13.6	11.7	13.4	–3.4	11.2	–7.2	–1.6	–4.7
Tl_2ZrSe_3	48.5	61.2	32.5	16.3	18.0	13.8	11.8	14.5	–3.4	13.0	–7.4	–0.4	–6.2
Tl_2ZrTe_3	38.7	48.4	31.8	17.6	18.0	13.6	10.8	13.9	–4.1	14.8	–8.1	0.6	–8.2

Elastic constants C_{11}, C_{22}, and C_{33} measure the resistance to linear compression in the x-, y-, and z-directions, respectively. All compounds resist to compression in y-direction better than that in the other directions, so the compressibility from higher to lower is $\beta_z > \beta_x > \beta_y$. As the atomic weight of the chalcogens increases from S to Te, the compressibility increases for the x- and y-directions. On the other hand, there is no significant change in the values along z-direction. The present C_{11} and C_{33} are higher than C_{44} and C_{66}. This indicates the weaker resistance to the unidirectional compression compared to the resistance to shear deformation.[39] It is known that the elastic constant C_{44} is the most important parameter indirectly guiding the indentation hardness of a material. The large C_{44} means a strong ability of resisting the monoclinic shear distortion in (100) plane. In the present case, C_{44} of Tl_2ZrTe_3 has the highest value.

3.3.2. Polycrystalline properties

The bulk modulus B (a resistance to shape change under pressure) and shear modulus G (a resistance to deformations upon shear stress)[40] have been obtained from the Voigt–Reuss–Hill approximations[41] by using the calculated elastic constants. The Young's modulus E and Poisson ratio ν are calculated through $E = 9GB/(G+3B)$ and $\nu = \frac{1}{2}\left[\left(B - \frac{2}{3}G\right)/\left(B + \frac{1}{3}G\right)\right]$, which are given in Table 5 with B/G ratio, Debye temperature, longitudinal, transverse, and average sound velocities. The calculated bulk moduli for the considered systems are smaller than 100 GPa, and hence these compounds may be classified as a soft material with high compressibility. As the atomic weight of the chalcogens increases of S to Te, the compressibility increases in the x- and y-axes too.

Table 5. Calculated bulk modulus B (GPa), isotropic shear modulus G (GPa), Young's modulus E (GPa), Poisson's ratio ν, B/G ratio, Vicker hardness H_v, (GPa) Debye temperature Θ_D, (K), and longitudinal, transverse and average sound velocities (ϑ_l, ϑ_t, ϑ_m, m/s).

Compound	B	G	E	ν	B/G	H_v	θ_D	ϑ_l	ϑ_t	ϑ_m
Tl_2HfS_3	22.3	14.6	36.0	0.23	1.53	2.9	158.2	2413	1427	1581
Tl_2HfSe_3	22.0	14.6	35.8	0.23	1.51	2.9	146.4	2304	1367	1514
Tl_2HfTe_3	20.9	13.6	33.4	0.23	1.54	2.6	133.9	2239	1321	1464
Tl_2ZrS_3	23.6	15.6	38.3	0.23	1.51	3.1	175.0	2669	1582	1752
Tl_2ZrSe_3	23.7	15.3	37.7	0.23	1.55	2.9	158.7	2516	1483	1643
Tl_2ZrTe_3	21.5	13.6	33.6	0.24	1.58	2.4	140.4	2366	1386	1536

Their shear moduli are almost similar to each other. However, since the large shear modulus is an indication of the more pronounced directional bonding between atoms.[42] It can generally be said that directional bonding of Tl_2ZrS_3 is more notable than that of the others due to its high value. On the other hand, a larger C_{44} elastic constant result with a larger shear modulus is not valid for our compounds.[43]

A greater Young's modulus indicates a stiffer material, it is a measure of the resistance against uniaxial tensions.[44] Tl_2ZrS_3 has the largest bond strength among the considered systems, resulting in more resistivity to any deformation. A ductile material can be accessed with the help of Pugh's ratio (B/G). Since all of the ratios are lower than 1.75, which is the critical starting value of ductility, all our considered systems show a brittle behavior.

The Poisson ratio is a measure of compressibility. when the Poisson ratio is close to 0.5, the material has tendency to be incompressible.[45] Here, the calculated Poisson ratio

is about 0.23, which indicates that these materials are less compressible and stable against elastic deformation.[46] The value of Poisson ratio is also indicative of the degree of directionality of the covalent bonding. The Poisson ratio is about 0.1, 0.25, and 0.33 for covalent, ionic, and metallic materials, respectively.[47] Since the values are about 0.23, ionic contribution in the intra-atomic bonding is dominant with no central interatomic forces for the considered structures due to the lower limit of 0.25 for the central force solids. According to Frantsevich rule, the critical value of Poisson ratio of material is 0.33. Frantsevich *et al.* indicated that if the Poisson ratio is less than 0.33, the materials show brittle behavior.[48] This supports our results from the analysis of Pugh's ratio (B/G).

The elastic and plastic properties of a material can be related to its hardness. The compounds are soft materials, since all of the calculated Vickers hardness values are lower than 10 GPa (see Table 5), as also supported by the bulk modulus values.

As an important fundamental parameter, the Debye temperature (θ_D) is closely linked to many physical properties of solids such as the specific heat and melting temperature. At low temperatures, the vibrational excitations originate entirely from acoustic vibrations. As a result, the Debye temperature calculated from elastic constants is the same as that determined from specific heat measurements for the low temperature values. Elastic constant data can be used for calculating the Debye temperature by estimating it from the average sound velocity (v_m).[49,50] Mostly for hard materials it is higher or vice versa.[51] All of the considered systems are soft materials due to their low Debye temperatures.

3.3.3. Elastic anisotropy

Elastic anisotropy affects many physical processes such as plastic deformation development in crystals, enhancement of positively charged defect mobility, microscale cracking, phonons in crystallites, etc.[52] The degree of anisotropy in the bonding between atoms in different planes (A1, A2, and A3) could be measured by means of the shear anisotropic factors. Any value smaller or greater than 1, which is the isotropy criterion of crystals, is the indication of shear anisotropy. In addition, we have also calculated the percentage elastic anisotropy of bulk and shear moduli. In these expressions, the zero value correlates to the elastic isotropy and the value of 100% pinpoints the largest elastic anisotropy. Our results are given in Table 6. As the atomic weight of chalcogens increases, while anisotropy increases for the values of A1, it decreases for the values of A3. Tl_2ZrSe_3 and Tl_2HfSe_3 can be thought as almost isotropic compounds for the values of A2. The calculated A_G value of all compounds is higher than the A_B values, indicating that shear anisotropy is greater than bulk anisotropy. It is obvious that Tl_2ZrTe_3 exhibits relatively high shear anisotropy, while Tl_2HfS_3 exhibits relatively high compressibility among the compounds.

Table 6. The calculated shear anisotropy factors (A1, A2, and A3) and the percentage of anisotropy in the bulk and shear (A_B and A_G).

Compound	A_1	A_2	A_3	A_B/%	A_G/%
Tl_2ZrS_3	1.05	0.80	0.53	8	8
Tl_2ZrSe_3	1.26	1.06	0.64	4	8
Tl_2ZrTe_3	1.64	1.42	0.83	2	11
Tl_2HfS_3	0.95	0.72	0.45	10	10
Tl_2HfSe_3	1.16	0.92	0.58	6	8
Tl_2HfTe_3	1.51	1.29	0.77	3	9

3.4. Transport properties

We have calculated the transport properties of the Tl_2MQ_3 compounds based on the Boltzmann transport equation under a rigid band and constant relaxation time approximations (RTA) which are very helpful in evaluating thermoelectric performance of materials based on theoretical band structure calculations,[53,54] i.e., the chemical potential shifts up or down from the intrinsic limit depending on the doping type and degree of doping and keeping the band structure unchanged.[55] In the rigid band approximation, the band structure is considered to be unaffected by doping, which only leads to change of the chemical potential. Boltzmann transport equations have a derivative of Fermi function with respect to the band structure and varies significantly within a small range near the chemical potential. So, in the calculations, instead of dependence of relaxation time on both the band index and the k vector direction, we have considered a direction independent τ, i.e., an almost constant relaxation time, which is a rational good approximation to express the transport coefficients.[56,57] Within RTA, the Seebeck coefficient can be calculated without any adjustable parameter.[58] However, the electronic conductivity has to be calculated with respect to the relaxation time and hence instead of calculating the absolute power factor ($S^2\sigma$), the power factor is calculated with respect to relaxation time ($S^2\sigma/\tau$).[58]

Within the constant relaxation time approximation, the value of relaxation time is fixed to be in the order of $\tau \sim 10^{-14}$ s, which is a typical value for semiconductors.[59,60] The variation of Seebeck coefficient of Tl_2HfSe_3 with temperature and concentration is depicted in Fig. 6. For this material, the maximum Seebeck coefficient is obtained for n-type doping and the optimal carrier concentration is 10^{17} cm^3.

The Seebeck coefficient of Tl_2HfSe_3 as a function of p-type and n-type carrier concentration at 300 K is shown in Fig. 7. The S of the p-type Tl_2HfSe_3 is positive, while that of the n-type is negative. The absolute S values decrease with the increase of carrier concentration, which means that one can obtain satisfactory S by tuning the carrier concentration. The absolute S of the n-type at lower carrier concentration is

larger than that of the p-type, however, the decrease scale is also larger. They both are close to zero at the carrier concentration of 10^{21} cm^{-3}, which implies that Tl_2HfSe_3 cannot be appropriate for thermoelectric application because the very small S will result in very small ZT.

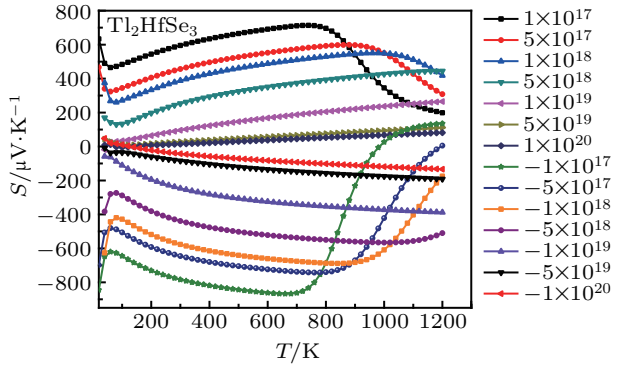


Fig. 6. The Seebeck coefficient of Tl_2HfSe_3 at different concentration (cm^{-3}) and temperature.

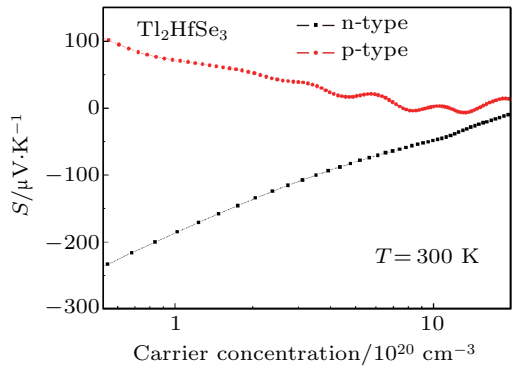


Fig. 7. The Seebeck coefficient of p-type and n-type Tl_2HfSe_3 as a function of carrier concentration at 300 K.

The calculated Seebeck coefficient (S), electrical conductivity (σ/τ), electronic thermal conductivity (k_e/τ), power factor ($S^2\sigma/\tau$), and ZT_{el} of Tl_2HfSe_3 as a function of chemical potential at carrier concentration 10^{17} cm^{-3} are plotted in Figs. 8–13.

The Seebeck coefficient is an important tool, which provides a sensitive test of the electronic structures of the materials in close proximity to the Fermi energy. Large values of Seebeck coefficient are desired for efficient TE devices. The calculated S of the titled compound as a function of μ at different temperatures is illustrated in Fig. 8. In the case of n-type doping, the Fermi level gets up-shifted towards the conduction band, resulting in a positive μ; while for p-type doping, the Fermi level shifts down towards the valence band, resulting in a negative μ. Assuming an energy independence of τ concludes a τ independence of Seebeck coefficient. Consequently, $S(T)$ dependency should be considered with respect to the carrier population, the intrinsic velocities, and density of states near the band gap rather than $\tau(T)$ dependence.[61] In the vicinity of Fermi level, the Seebeck coefficient exhibits two pronounced peaks for n-/p-types. The investigated material gives the highest S at 300 K, which means that this material has good thermoelectric performance. The maximum value of Seebeck coefficient decreases with increase in temperature. These values are 1104.23 μV/K and −985.32 μV/K for p- and n-type Tl_2HfSe_3, respectively. We should highlight that the critical points of Seebeck coefficient for p- and n-type Tl_2HfSe_3 are between 0.26 eV and 0.36 eV where the material exhibits good thermoelectric properties, while beyond these points, S drops rapidly to zero. To see the effect of the GGA + HSE06 functional on Seebeck coefficient calculations at 300 K, we present Fig. 9. From this figure, it can be concluded that HSE06 functional on GGA increases the Seebeck coefficient from −985.32 μV/K to −1980.9 μV/K and shifts right at the higher Fermi level.

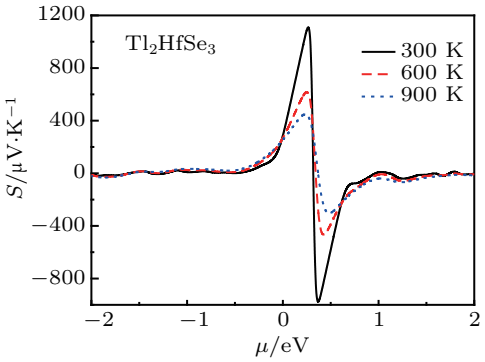


Fig. 8. The calculated Seebeck coefficient as a function of chemical potential at 300 K, 600 K, and 900 K for Tl_2HfSe_3.

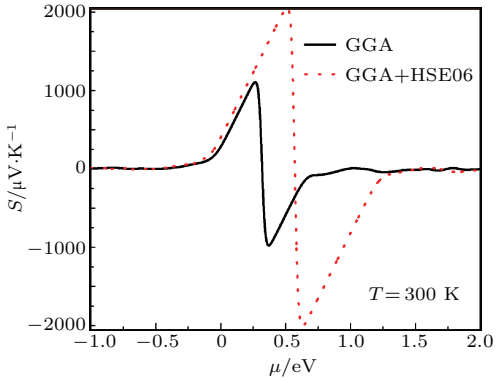


Fig. 9. The calculated Seebeck coefficient as a function of chemical potential at 300 K for Tl_2HfSe_3.

Electrical conductivity σ in units of τ has been calculated as a function of the chemical potential μ at three temperatures (300 K, 600 K, and 900 K) given in Fig. 10. It can be seen from Fig. 10 that the electrical conductivity is minimum between 0–0.66 eV and increases as the chemical potential increases. So desired values of electrical conductivity could be obtained with the change in the chemical potential. The σ/τ value of Tl_2HfSe_3 has two apparent peaks at $\mu = -1.61$ eV (nearly 1.53×10^{20} $(\Omega\cdot m\cdot s)^{-1}$ for n-type) and $\mu = 1.83$ eV, increases smoothly near the region $\mu = 0.27$ eV.

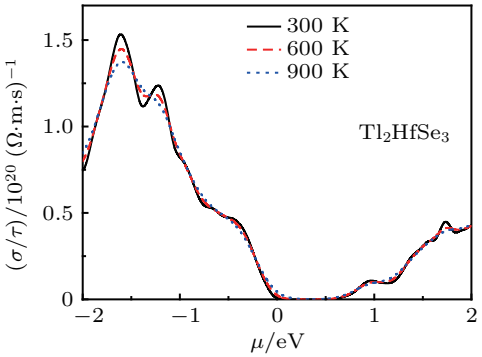


Fig. 10. The calculated electrical conductivity (in units of relaxation time τ) as a function of the chemical potential at 300 K, 600 K, and 900 K for Tl_2HfSe_3.

While lattice vibrations are mostly subject to the heat conduction in semiconductors, free electrons are commonly the key of thermal conductivity in metals.[62] The thermal conductivity involves two parts as $k = k_e + k_l$, where electrons and holes in k_e and phonons in k_l are responsible for heat transport. The total thermal conductivity in metals could be evenly neglected, because its percentage is less than 2 causing from the lattice part.[63,64] We have obtained k_e/τ (in units of τ) as a function of μ at temperatures 300 K, 600 K, and 900 K using energy independent relaxation time approximation like before with the results given in Fig. 11. Minimum values of k_e/τ are obtained with μ between 0.0 eV and 0.7 eV, having the maximum efficiency for Tl_2HfSe_3. The maximum values of the electronic thermal conductivity in units of τ are obtained with μ between -1.5 eV and 2.0 eV, where the maximum values of k_e/τ for n-types are lower than those for p-types. Also, it is concluded from Fig. 11 that the thermal conductivity increases with temperature because free electrons gain more energy. Electronic thermal conductivity per second for positive chemical potential is smaller than that for negative chemical potential.

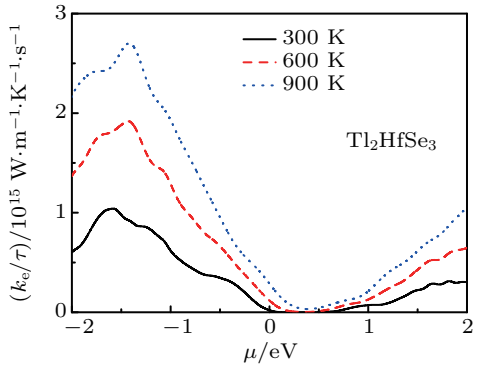


Fig. 11. Electronic thermal conductivity k_e as a function of chemical potential at 300 K, 600 K, and 900 K for Tl_2HfSe_3 (the zero at low T corresponds to the undoped systems).

It is important to increase the value of P as much possible as without increasing the total thermal conductivity k.[65] The P is given in Fig. 12 for temperatures 300 K, 600 K, and 900 K. The power factor is the minimum near the Fermi level and beyond increases rapidly to form two pronounced peaks located at $\mu = -0.1$ eV and 0.72 eV, for p-/n-type doping of Tl_2HfSe_3. The maximum value of power factor is 0.335×10^{12} W/m·s·K^2 for p-type doping at 900 K, thereafter it decreases with decreasing the temperature.

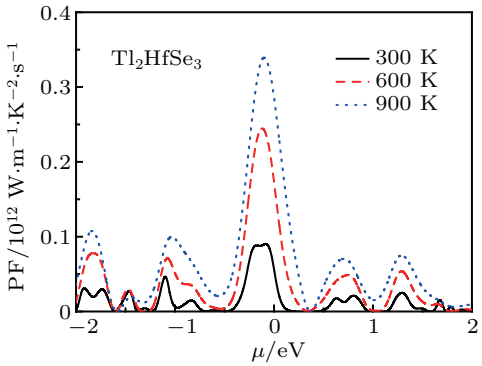


Fig. 12. Power factor of Tl_2HfSe_3 at 300 K, 600 K, and 900 K as a function of the chemical potential.

In the figure of merit calculations, we have only considered the electronic part of ZT because of not know anything (theoretically) about the lattice thermal conductivity. So, we define $(ZT)_{el} = S^2\sigma T/k_{el}$, which depends only on the electronic properties and $ZT = (ZT)_{el}\frac{1}{(1+k_l/k_{el})}$. Since $(1+k_l/k_{el})$ is greater than 1, $ZT < (ZT)_{el}$.

The $(ZT)_{el}$ provides an upper limit to the figure of merit. It is well known that there are two types of k_{el}, as $k_{el,J}$ at $\boldsymbol{J} = 0$ and as $k_{el,E}$ at $\boldsymbol{E} = 0$. Extremely small thermopower value in metals or strongly degenerate semiconductors makes these two electronic thermal conductivities nearly the same.[55] Whereas their values are completely different in good thermoelectric possessing large thermopower value.[66] For simplicity in this paper, we will calculate $(ZT)_{el}$ considering only $k_{el,E}$, and plot its graph as a function of the chemical potential for 300 K, 600 K, and 900 K in Fig. 13.

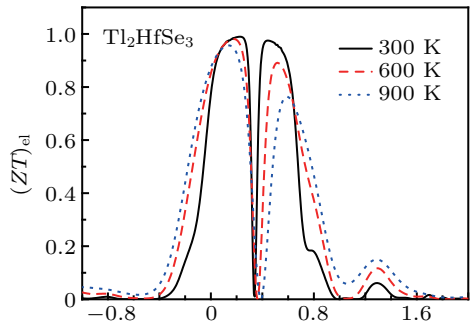


Fig. 13. Figure of merit $(ZT)_{el}$ for Tl_2HfSe_3.

Seebeck coefficient S, electrical conductivity σ/τ, power factor P, and $(ZT)_{el}$ as a function of different temperature with a doping concentration of 10^{17} cm^{-3} are given in Figs. 14(a)–14(d) for the studied compounds. It is clear that the Seebeck coefficient is considerably varying with temperature. The Seebeck coefficient of Tl_2ZrTe_3 and Tl_2HfTe_3 begins from

127 μV/K and decreases up to 300 K, and then rises exponentially for both compounds, owing to the rise in temperature up to 600 K, and then at higher temperature shows the slightly constant rate. The S values for Tl_2ZrSe_3, Tl_2HfSe_3, and Tl_2ZrS_3 decrease up to 450 K, 700 K, and 750 K, respectively, and then increase for higher temperatures. At 750 K, for the Tl_2ZrS_3 compound, the maximum Seebeck coefficient is 473.6 μV/K, which endorses that this compound has potential applications in thermoelectric devices. The variation of electrical conductivity is shown in Fig. 14(b), per relaxation time with temperature. It can be seen obviously from Fig. 14(b) for Tl_2ZrTe_3 and Tl_2HfTe_3 that the electrical conductivity is almost linear with temperature up to 400 K, while for higher temperatures increases linearly. At 1000 K, the highest obtained electrical conductivity for the Tl_2ZrTe_3 compound is 0.04858×10^{20} $(\Omega\cdot\text{ms})^{-1}$. The variation of thermal conductivity is shown in Fig. 14(c), per relaxation time with temperature and all compounds increase exponentially with temperature. The $(ZT)_{el}$ for Tl_2ZrTe_3, Tl_2HfTe_3, and Tl_2ZrSe_3 increase to 0.8 till 200 K and then decrease for higher temperatures, which is enough for practical applications. According to Ref. [28] for Tl_2ZrTe_3, they have found ZT value of 0.18 at 420 K, which is higher than our value (0.044 at 400 K). The highest value of $(ZT)_{el}$ is obtained for Tl_2HfSe_3 as 0.9 at 600 K as shown in Fig. 14(d).

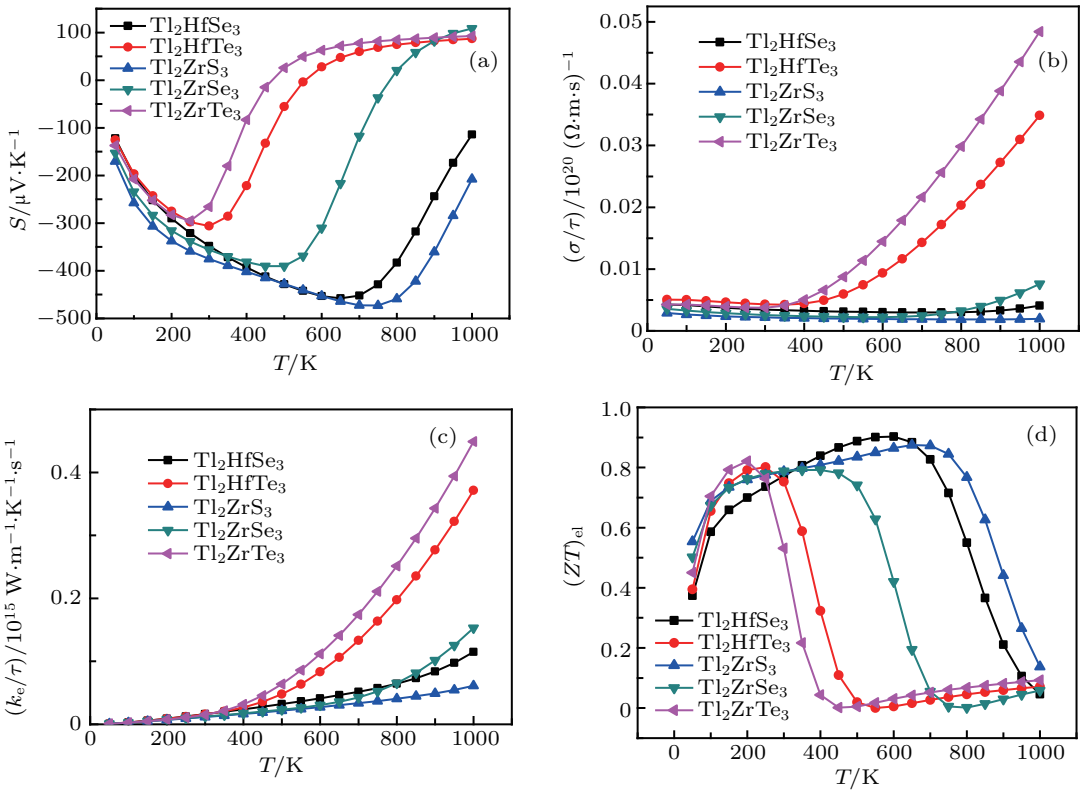


Fig. 14. The calculated (a) Seebeck coefficient, (b) electrical conductivity (in units of relaxation time τ) (c) thermal conductivity (in units of relaxation time τ), and (d) figure of merit $(ZT)_{el}$ as a function of temperature for Tl_2MQ_3 (M = Hf, Zr; Q = S, Se, Te).

In order determine the thermoelectric figure of merit of Tl_2HfSe_3, the thermal conductivity including the k_l of lattice and the k_e of electron needs to be calculated. The lattice thermal conductivity k_l equation derived by Slack[67] is given as

$$k_l = A\frac{M\delta\theta_D^2}{\gamma n^{2/3}T}. \tag{2}$$

Here M is the average atomic weight, δ^3 is the average volume of the mass equivalent one atom in the primitive unit cell, T is the absolute temperature, n is the number of atoms per unit cell, γ is the Gruneisen parameter,[68] and A is a coefficient depending upon γ. The Gruneisen parameter is calculated using the following Poison ratio (ν) equation:

$$\gamma = \frac{3(1+\nu)}{2(2-3\nu)}, \tag{3}$$

$$A(\gamma) = \frac{5.720\times0.849\times10^7}{1-\frac{0.514}{\gamma}+\frac{0.228}{\gamma^2}}. \tag{4}$$

At room temperature, the computed value of γ using Eq. (3) is 1.408. The k_l for Tl_2HfSe_3 is evaluated as 2.975 W/mK at 300 K.

For Tl_2HfSe_3, at T = 300 K, using relaxation time $\tau = 10^{-14}$ s, the electronic thermal conductivity and electrical conductivity are obtained to be $k_e = 6.509\times10^{-3}$ W/m·K and $\sigma = 36.55$ $(\Omega\cdot\text{m})^{-1}$. Finally, the figure of merit can be obtained from the following equation as 2.1764×10^{-3} at 300 K

which is very low compared to materials with good thermoelectric performance,

$$ZT = \frac{S^2\sigma T}{k_e + k_l}. \quad (5)$$

Therefore, Tl_2HfSe_3 should not be a kind of materials with good thermoelectric performance at 300 K.

4. Conclusion

We have studied the structural, mechanical, electronic, and thermoelectrical properties of monoclinic Tl_2MQ_3 (M = Zr, Hf; Q = S, Se, Te) compounds by performing first-principles calculations. The calculated lattice parameters are in agreement with the available experimental data. The other original features of the present calculations involve the elastic, mechanical, and thermoelectrical results, which have not been considered previously. The analysis of the elastic constants indicates the mechanical stability and that the compounds have a brittle and soft nature with respect to the B/G (~ 1.5), Poisson's ratio (~ 0.23), and H_v (~ 3 GPa) criteria. All studied systems are semiconductors in nature, which is also supported by the computed band structures, having an indirect band gap except for the Tl_2ZrS_3 compound. The total and projected densities of states of the studied compounds indicate that while Q (S, Se, and Te) elements are dominant in the conduction band, the leading elements of the valance band are M (Hf and Zr). The electronic transport properties are calculated as a function of the chemical potential and the highest value for $(ZT)_{el}$ is tabulated for Tl_2HfSe_3 as 0.9 at 600 K. But using experimental value of electrical conductivity for Tl_2HfSe_3 at 300 K, ZT is obtained to be 2.176×10^{-3} which is very low. We hope that the current theoretical prediction will stimulate extensive experimental synthesis thermoelectric materials.

Acknowledgment

The numerical calculations reported in this paper were performed at TUBITAK ULAKBIM, High Performance and Grid Computing Center (TRUBA resources) and Aksaray University, Science and Technology Application and Research Center HPC System.

References

[1] Gerbi A, Buzio R, Kawale S, Bellingeri E, Martinelli A, Bernini C, Tresca C, Capone M, Profeta G and Ferdeghini C 2017 *J. Phys. Condens.: Matter* **29** 485002
[2] Ali M 2017 *J. Supercond Nov Magn.* **30** 3409
[3] Xu M, Jakobs S, Mazzarello R, Cho J Y, Yang Z, Hollermann H, Shang D, Miao X, Yu Z, Wang L and Wuttig M 2017 *J. Phys. Chem. C* **121** 25447
[4] Komisarchik G, Gelbstein Y and Fuks D 2017 *Intermetallics* **89** 16
[5] Wei K, Khabibullin A R, Stedman T, Woods L M and Nolas G S 2017 *J. Appl. Phys.* **122** 105109
[6] Wang H, Yuan H, Sae Hong S, Li Y and Cui Y 2015 *Chem. Soc. Rev.* **44** 2664
[7] Li L, David S P, Clarina R C and Athena S S 2016 *Physica C* **531** 25
[8] Aliev Z S Zúñiga F J Koroteev Y M Breczewski T Babanly N B Amiraslanov I R Politano A Madariaga G Babanly M B Chulkov E V 2016 *J. Solid State Chem.* **242** 1
[9] Guo Q, Chan M, Kuropatwa B A and Kleinke H 2013 *Chem. Mater.* **25** 4097
[10] Toberer E S, May A F and Snyder G J 2010 *Chem. Mater.* **22** 624
[11] Banik A, Shenoy U S, Anand S, Waghmare U V and Biswas K 2015 *Chem. Mater.* **27** 581
[12] Zhao L D, Hao S, Lo S H, Wu C I, Zhou X, Lee Y and Kanatzidis M G 2013 *J. Am. Chem. Soc.* **135** 7364
[13] Zhao L D, Zhang X, Wu H, Tan G, Pei Y, Xiao Y, Chang C, Wu D, Chi H, Zheng L, Gong S, Uher C and He J M G 2016 *J. Am. Chem. Soc.* **138** 2366
[14] Guo Q, Assoud A and Kleinke H 2014 *Adv. Energy Mater.* **4** 1400348
[15] Li J F, Liu W S, Zhao L D and Zhou M 2010 *NPG Asia Mater.* **2** 152
[16] Karthikeyan N, Ghanta S, Misra S, Jaiganesh G, Jana P P and Sivakumar K 2017 *J. Alloys Compd.* **729** 303
[17] Orabi R A R, Boucher B, Fontaine B, Gall P, Candolfi C, Lenoir B, Gougeon P, Halet J F and Gautier R 2017 *J. Mater. Chem. C* **5** 12097
[18] Li W, Lin S, Zhang X, Chen Z, Xu X and Pei Y 2016 *Chem. Mater.* **28** 6227
[19] Heinke F, Eisenburger L, Schlegel R, Schwarzmüller S and Oeckler O 2017 *Anorg. Allg. Chem.* **643** 447
[20] Li G, Aydemir U, Duan B, Agne M T, Wang H, Wood M, Zhang Q, Zhai P, Goddard I I I W A and Snyder G J 2017 *ACS Appl. Mater. Interfaces* **9** 40488
[21] McGuire M A, Schmidt A M, Gascoin F, Snyder G J and DiSalvo F J 2006 *J. Solid State Chem.* **179** 2158
[22] Assoud A, Shi Y, Guo Q and Kleinke H 2017 *J. Solid State Chem.* **256** 6
[23] Shi Y, Assoud A, Sankar C R and Kleinke H 2017 *Chem. Mater.* **29** 9565
[24] Guo Q and Kleinke H 2015 *J. Alloys Compd.* **630** 37
[25] Sankar C R and Aswathy V S 2018 *Inorg. Chem. Front.* **5** 1553
[26] Sankar C R, Bangarigadu-Sanasy S, Assoud A and Kleinke H 2010 *J. Mater. Chem.* **20** 7485
[27] Kurosaki K, Uneda Muta H and Yamanaka H 2004 *J. Alloys Compd.* **376** 43
[28] Sankar C R, Guch M, Assoud A and Kleinke H 2011 *Chem. Mater.* **23** 3886
[29] Sankar C R, Kuropatwa B A, Assoud A and Kleinke H 2012 *Dalton Trans.* **41** 9646
[30] Kresse G and Hafner J 1993 *Phys. Rev. B* **47** 558
[31] Kresse G and Furthmüller J 1996 *Comput. Mater. Sci.* **6** 15
[32] Kresse G and Hafner J 1994 *Phys. Rev. B* **49** 14251
[33] Kresse G and Furthmüller J 1996 *Phys. Rev. B* **54** 11169
[34] Blöchl P E 1994 *Phys. Rev. B* **50** 17953
[35] Perdew J P, Burke K and Ernzerhof M 1996 *Phys. Rev. Lett.* **77** 3865
[36] Monkhorst H J and Pack J D 1976 *Phys. Rev. B* **13** 5188
[37] Madsen G K H and Singh D J 2006 *Comput. Phys. Commune.* **175** 67
[38] Singh D J 2001 *Semiconduc. Semimet.* **70** 125
[39] Murnaghan F D 1944 *Proc. Natl. Acad. Sci. USA* **30** 244
[40] Jong D, Chen M, Angsten W, Jain T, Notestine A, Gamst R, Sluiter A, Krishna M, Ande van der Zwaag C, Plata S, Toher J J, Curtarolo C, Ceder S, Persson G, Asta K A and Charting M 2015 *Sci. Data* **2** 150009
[41] Page Y L and Saxe P 2002 *Phys. Rev. B* **65** 104104
[42] Li S, Ju X and Wan C 2014 *Comput. Mater. Sci.* **81** 378
[43] Yu R, Chong X, Jiang Y, Zhou R, Yuan W and Feng J 2015 *RSC Adv.* **5** 1620
[44] Hill R 1952 *Proc. Phys. Soc. London* **65** 349
[45] Mott P H, Dorgan J R and Roland C M 2008 *Journal of Sound and Vibration* **312** 572
[46] Sohafiq M, Ahmad I and Asodobadi S J 2014 *J. Appl. Phys.* **1 6** 103905
[47] Haines J, Leger J M and Bacquillan G 2001 *Ann. Rev. Mater. Res.* **31** 1
[48] Ravindran P, Fast L, Korzhavyi P A and Johansson B 1998 *J. Appl. Phys.* **84** 4891
[49] Deligoz E, Ozisik H B, Colakoglu K and Ciftci Y O 2014 *Mater. Sci. Technol.* **30 7** 842
[50] Chattaraj D, Majumder C and Dash S 2014 *J. Alloys Compd.* **615** 234
[51] Frantsevich I N, Voronov F F and Bokuta S A 1982 *Elastic Constants and Elastic Moduli of Metals and Insulators: Handbook* (Naukova Dumka: Kiev)

[52] Johnston I, Keeler G, Rollins R and Spicklemire S 1996 *Solid State Physics Simulations, The Consortium for Upper-Level Physics Software* (New York: John Wiley)

[53] Schreiber E, Anderson O L and Soga N 1973 *Elastic constants and their measurements* (New York : McGraw-Hill)

[54] Zhao E, Wang J and Wu Z 2010 *J. Comput. Chem.* **31** 2883

[55] Miao N, Sa B, Zhou J and Sun Z 2011 *Comput. Mater. Sci.* **50** 1559

[56] Chaput L, Pecheur P, Tobola J and Scherrer H 2005 *Phys. Rev. B* **72** 085126

[57] Bilc D I, Mahanti S D and Kanatzidis M G 2006 *Phys. Rev. B* **74** 125202

[58] Ciftci Y O and Mahanti S D 2016 *J. Appl. Phys.* **119** 145703

[59] Guo R, Wang X, Kuang Y and Huang B 2015 *Phys. Rev. B* **92** 115202

[60] Yu P Y and Cordona M 2010 *Fundamentals of Semiconductors; Graduate text in Physics* (Berlin: Springer)

[61] Gzyl H 1982 *J. Stat. Phys.* **29** 617

[62] Scheidemantel T J, Ambrosch-Draxl C, Thonhauser T, Badding J V and Sofo J O 2003 *Phys. Rev. B* **68** 125210

[63] Nasr T B, Maghraoui-Meherzi H and Kamoun-Turki N 2016 *J. Alloys Compd.* **663** 123

[64] Kong F, Hu Y, Hou H, Liu Y, Wang B and Wang L 2012 *J. Solid State Chem.* **196** 511

[65] Rabin O, Lin Y M and Dresselhaus M S 2001 *Appl. Phys. Lett.* **79** 81

[66] Tritt T M 2004 *Thermal Conductivity: Theory, Properties, and Aplications* (New York: Kluwer Academic/PLENUM Publishers) p. 75

[67] Kittel C 2004 *Introduction to Solid State Physics* (8th Edn.) (Hoboken: John Wiley & Sons) p. 156

[68] Bilc D I, Hautier G, Waroquiers D, Rignanese G M and Ghosez P 2015 *Phys. Rev. Lett.* **114** 136601